Renewable Energy 99 (2016) 1227–1234

Contents lists available at ScienceDirect

Renewable Energy

journal homepage: www.elsevier.com/locate/renene

Experimental investigations of the Hydro-Spinna turbine performance

R. Rosli*, R. Norman, M. Atlar

School of Marine Science and Technology, Armstrong Building, Newcastle University, Newcastle upon Tyne, NE1 7RU, United Kingdom

ARTICLE INFO

Article history:
Received 1 August 2015
Received in revised form
9 August 2016
Accepted 11 August 2016
Available online 19 August 2016

Keywords:
Tidal current
Tidal turbine
Turbine design
Horizontal axis
Power
Performance

ABSTRACT

A unique tidal turbine, "Hydro-Spinna", is introduced. The Hydro-Spinna consists of three cardioidal blades spiralling around a common horizontal shaft. A 500 mm diameter model was manufactured and its performance investigated in the towing tank facility of Newcastle University. The main objective of these experiments was to investigate the hydrodynamic efficiency of Hydro-Spinna with a view to improve the design by collecting data for use in numerical optimization. Considering its flexible operating characteristics the model turbine was tested at different immersion depths and in the half-submerged condition. The power coefficient of the turbine reached a value of almost 0.3 at a tip speed ratio of 2.2 in the fully submerged condition. The turbine had a higher power coefficient in shallow immersion and half submerged condition. The drag coefficient on the whole system decreased with increasing TSR contrary to conventional turbines. The turbine was observed to start rotating at low flow velocities, down to 0.15 m/s. In the study, although the turbine presents a relatively low power coefficient compared to that of competitive turbines, its unique adaptability of immersion depth, including the partially submerged condition, low starting flow velocity and rotational speed offer an interesting prospect for a range of applications.

1. Introduction

Persisting environmental concerns along with the volatile nature of the fossil fuel economy reinforce the need to search further for sustainable alternative energy resources. The world's oceans which cover 71% of the earth's surface offer an array of marine energy opportunities with the potential to be exploited. In the UK alone, wave and tidal energy resources have been identified as being able to meet 20% of the energy requirements [1]. Tidal energy offers more opportunities due to its high predictability; unlike the less predictable waves, tides result from the regular gravitational interaction between the earth and the moon.

The traditional way of harvesting energy from tides is by means of a tidal barrage, exploiting the potential head available in the water and operating similar to a hydropower plant [2]. An alternative method is to extract the kinetic energy from the flow using tidal current turbines. The wind energy industry has been successful in establishing the generic design of horizontal axis turbine as the optimal configuration for energy extraction. Due to the similarity of wind and tidal flow, both being fluids, the horizontal axis turbine concept is the most commonly adopted format in the tidal energy industry.

A horizontal axis turbine is used to extract energy from the kinetic component of a moving fluid and the design of the turbine blade plays a very important role in the efficiency of the turbine. Tidal ranges and velocities vary depending on geographical location, land and seabed topography, with a peak velocity between 2 and 3 m/s considered as an economically viable site for extracting tidal energy [3]. Typically at such a site the tidal velocity ranges between 2 and 2.5 m/s during neap tide and 3.5–4 m/s during spring tide [4]. At certain locations, tidal velocities can reach up to 5 m/s as the tidal flow is amplified by geographical constraints such as narrow straits or headlands [5].

The maximum limit on the power that can be extracted from the fluid flow is 59% according to the Betz Theory [6]. The power available in the fluid flow is shown in equation (1).

$$P_{av} = \frac{1}{2}\rho A U^3 \tag{1}$$

where ρ is the density of the fluid, A is the swept area of the turbine and U is the flow velocity.

Wind turbines require relatively large diameters to extract the energy effectively from the flow however, the density of water is

* Corresponding author.
E-mail address: h.r.haji-rosli@newcastle.ac.uk (R. Rosli).

http://dx.doi.org/10.1016/j.renene.2016.08.034
0960-1481/

approximately 800 times higher than that of air, hence tidal turbines would have significantly smaller diameters for the same power rating. The power available in the flow is proportional to the velocity cubed, as shown in equation (1), so a fluctuating flow velocity will greatly affect the power. However, the tidal velocity is more predictable and fluctuates less compared to wind velocity. The velocity of a tidal stream is lower than the velocity of wind, therefore tidal turbines operate at slower rotational speeds as the energy content is greater in a tidal flow than in wind, a tidal turbine is subjected to higher loading than a wind turbine which requires a robust system.

Operation of tidal turbines can generate noise that may disturb the acoustic balance of the natural environment they are deployed in Ref. [7]. In the case where they are installed near the seabed, in shallow waters, they may increase the risk of scouring as reported in Ref. [8]. In addition, tidal turbines are prone to cavitation, that may be increased by the action of wave particle motions, causing the turbine blade to erode as well as radiating noise hence compromising its hydrodynamic integrity and further impacting on the marine environment [7,8]. On a similar note free surface effects due to waves and the turbine's own operation affect its energy production [9–11].

Most established tidal current devices are based on the conventional horizontal axis turbine generally adopted in the wind industry. Established horizontal axis tidal current energy, such as SeaGen [12] put the emphasis on the reliability and adaptability of such a design for tidal energy. Various other devices are also being tested at the European Marine Energy Centre (EMEC) reflecting the steady progress in the marine energy industry in the region. A significant amount of work has been done to study the performance of tidal current turbines at various working and flow conditions as well as the wake profiles [9,13–15]. Vertical axis tidal turbines and other unconventional tidal current devices have also been developed and investigated to harness the energy from tides [1,16–19].

A working novel marine current turbine design is presented in this paper including an experimental investigation into the power extraction capability of this turbine. The "*Hydro-Spinna*", which is the name given to the device by its inventor based on his wind spinner activity and observation [27], offers an innovative horizontal axis concept design for the tidal current energy industry. The unique design of the Hydro-Spinna is presented in Section 2 including its geometrical definition through analytical equations. The experimental set-up and tests for the evaluation of the power extraction performance are presented in Section 3. The performance results are investigated at different immersion depths over a range of operating tip speed ratio (TSR) and results are discussed in Section 4. Finally, Section 5 reports on the conclusions of the study.

2. Hydro-Spinna turbine

2.1. Turbine design

The Hydro-Spinna is a three cardioidal helicoidal bladed turbine which extracts energy from the tidal stream by aligning itself in the direction of the flow. A cardioid is a geometrical shape that follows the polar x-y coordinates of a circle. However, in the case of a circle where the radius is constant at every swept angle θ, the radius of the cardioid varies with angle, as presented in Fig. 1, and is defined as $r = a(1 - \cos\theta)$ where a is the scaling factor and $0 < \theta < 2\pi$. The plan form of the blade in the x-y direction is formed by creating two concentric cardioids as shown in Fig. 2.

Two generations of the Hydro-Spinna turbine have previously been designed, maintaining the basic cardioid leading edge design of the blade [20,21]. The first generation developed has a cardioid

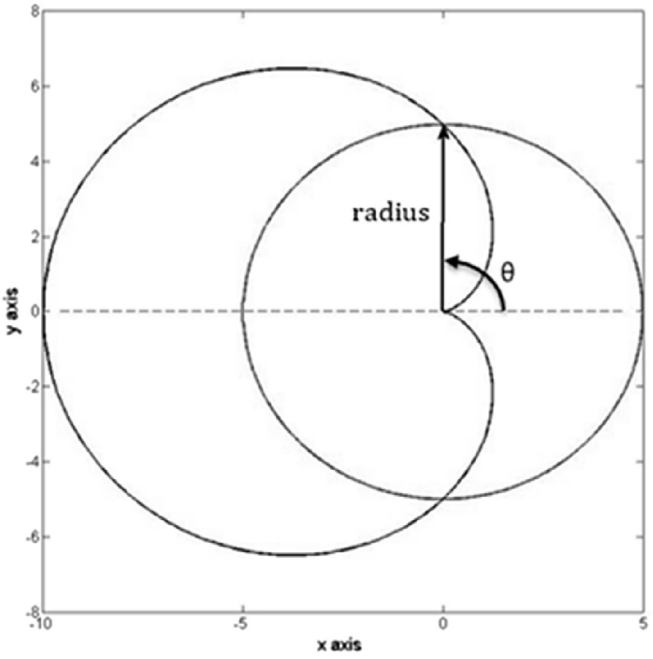

Fig. 1. The basic cardioid geometry and comparison of the cardioid shape (scaling factor a = 5) with a circle of radius = 5 for $0 < \theta < 2\pi$.

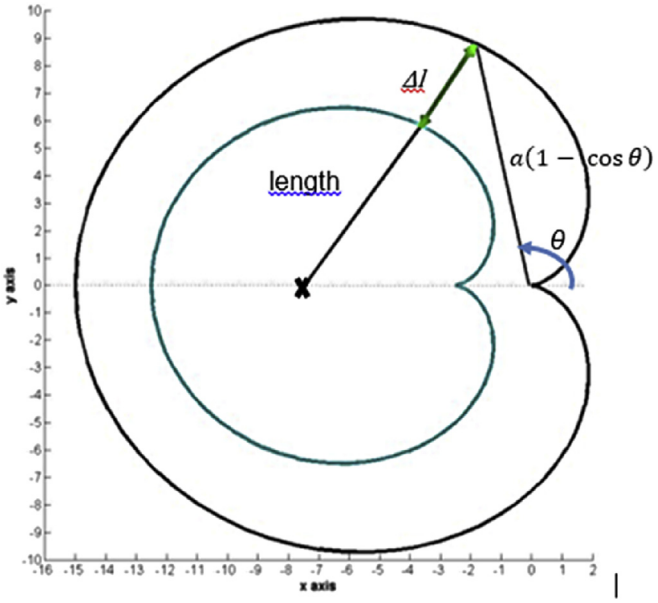

Fig. 2. The planform view of a Hydro-Spinna blade. The chord length of the blade, Δ*l*, is the length from the leading to trailing edge at the same angle θ from the designated centre **x**.

leading and trailing edge with equal chord length throughout the blade circumference while the second generation exhibits a circular trailing edge profile. The third generation turbine investigated in this paper is a modified version of the first generation and is further defined in the following.

The third generation turbine has cardioidal leading and trailing edges. The design of the turbine is developed in a mathematical form for simplicity of design and construction. The scaling factor ratio of the trailing to the leading cardioid is 1.5. The offset of the leading and trailing cardioid surfaces are given in equation (2–4),

while pitch angle, β, of the surface at any radius is given by equation (5).

$$x = a(1 - \cos\theta)\cos\theta \quad (2)$$

$$y = a(1 - \cos\theta)\sin\theta \quad (3)$$

$$z = p\theta \quad (4)$$

$$\beta = \tan^{-1}\left[\frac{\Delta Z}{\Delta l}\right] \quad (5)$$

where a is the cardioid scaling factor, θ is the swept angle, p is the pitch length of the turbine, ΔZ is the axial distance between the trailing and leading edge, and Δl is the chord length.

As each blade is spiraled around the hub along its longitudinal axis (z-axis), the blade meets the hub at two points, named the upstream and downstream end. The pitch length of the turbine *(p)* is the distance between the upstream and downstream end of the hub where the blade completes one helicoidal cycle in the axial fluid flow direction along the z-axis. The hub radius of the third generation device is 20% of the turbine diameter as illustrated in Fig. 3.

2.2. Hydro-Spinna model

The Hydro-Spinna has a unique design and key parameters need to be clearly defined. The diameter of the turbine (D) is defined as the diameter of the cross sectional area swept by the turbine. The pitch length (p) and chord (Δl) as described earlier are shown in Fig. 3 while the blade shape for the third generation device used an aerodynamic NACA0015 profile cross-section for its symmetrical and thick profile that will give structural stability to the blade.

The Hydro-Spinna model tested in the towing tank has a diameter of 500 mm with a pitch to diameter ratio of 0.42 and hub diameter of 100 mm. The model was manufactured from polymers using a 3-D printer as shown in Fig. 4. The radial distribution of the blade section details are given in Table 1:

3. Experimental set up and tests

3.1. Test facility and limitations

Tests were carried out in the Towing Tank facility at Newcastle University. The tank has the following dimensions while its further details can be found in Ref. [22]:

Tank length	37 m
Width	3.7 m
Depth	1.25 m
Maximum carriage velocity	3 m/s

Although the towing carriage can be driven up to a maximum speed of 3 m/s, the rotational speed of the turbine was regulated by a 1 Nm Magtrol HB-140M-2 magnetic brake. The turbine model therefore was tested up to a maximum carriage velocity of 0.9 m/s including tests at 0.5 and 0.7 m/s. This was due to the limitation of the brake capacity of 1 Nm that was insufficient to control the turbine rotation for lower TSR at higher flow velocities. A full range of tip speed ratio tests was only obtained at the minimum carriage velocity of 0.5 m/s.

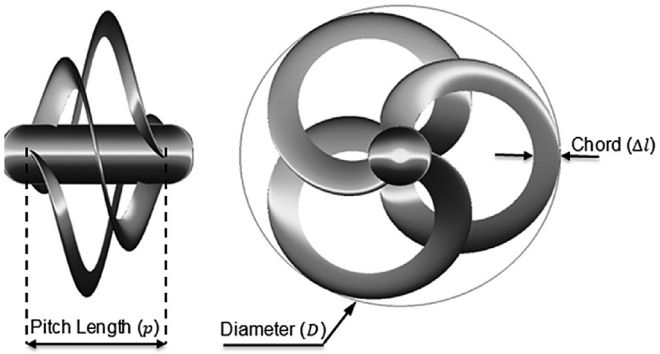

Fig. 3. Hydro-Spinna parameters defined.

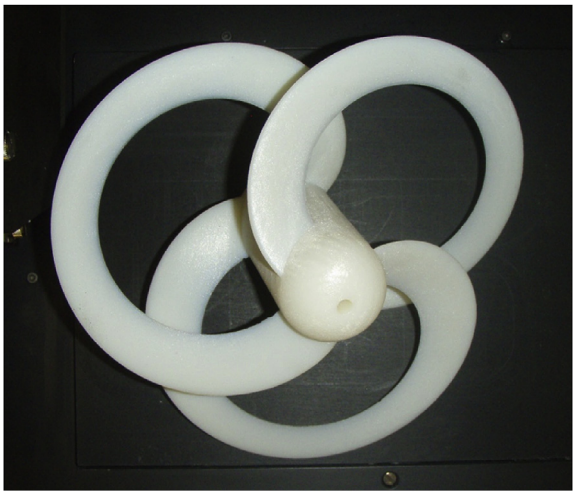

Fig. 4. The 3-D printed Hydro-Spinna turbine.

Table 1
Specification of the Hydro-Spinna model with the pitch angle and chord length defined at each cardioid radius.

Cardioid angle, θ	Cardioid Radii (mm)	Pitch angle (°) β	Chord (mm) Δl
0	0	50.2	65.1
30	16.7	41.8	62.5
60	62.5	31.1	64.4
90	125.0	23.0	64.0
120	187.5	16.8	57.6
150	233.3	10.1	47.3
180	250.0	0	41.7
210	233.3	−10.1	47.3
240	187.5	−16.8	57.6
270	125.0	−23.0	64.0
300	62.5	−31.1	64.4
330	16.7	−41.8	62.5
360	0	−50.2	65.1

3.2. Test set up

The Hydro-Spinna was supported by a front and back (main) struts to distribute the weight of the turbine as shown in Fig. 5. The front strut was introduced to support the weight of the turbine as well as to strengthen the entire assembly against the unsteady effects of the thrust and torque on the blades. Mechanical power was transmitted from the turbine via a pulley system to a shaft drive above the water level attached to the carriage rig.

As shown in Figs. 5 and 6, the shaft drive was connected to the

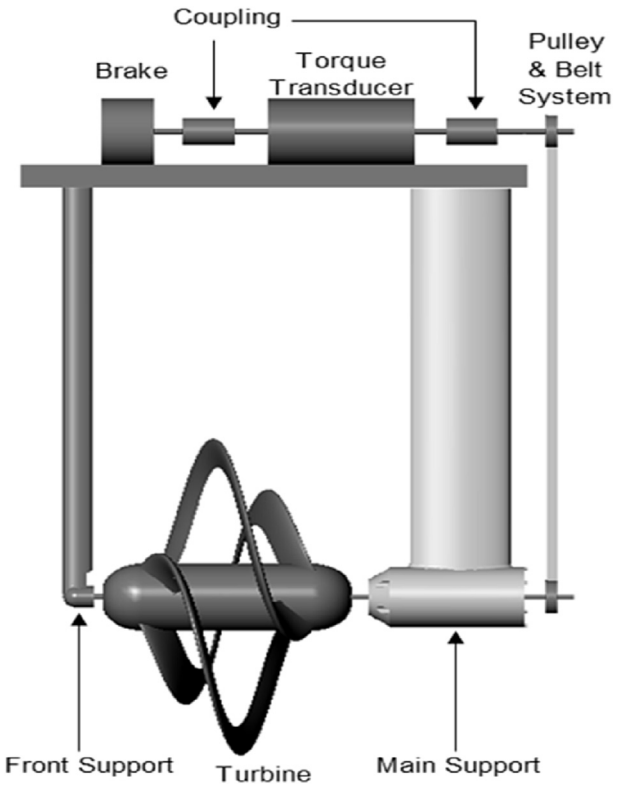

Fig. 5. Illustration of the turbine set up for the towing tank test.

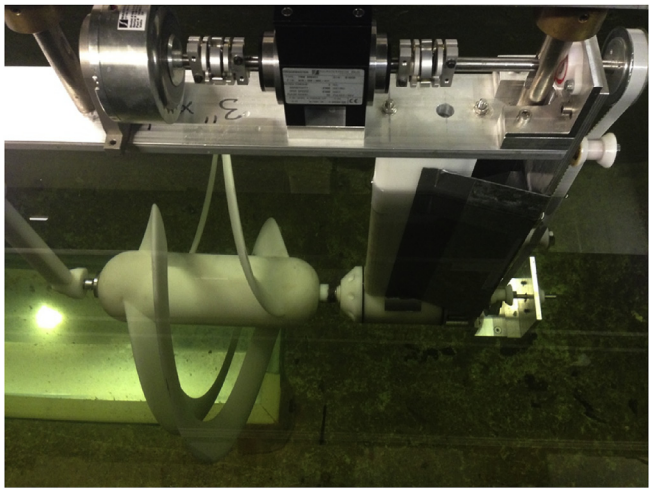

Fig. 6. The Hydro-Spinna experimental set up in the towing tank facility.

1Nm rated brake and a torque transducer to control the rotational speed of the turbine, and measure the torque and rotational speed, respectively. The thrust on the turbine alone was not measured. However, the overall turbine system was attached to a carriage equipped with load cells to measure the total drag force of the turbine and both front and main supports.

Experimental data was recorded every 0.01 s where 10 s of data were taken giving a total of 1001 samples. A total of 3 runs were carried out for each condition. The standard deviation and standard error with 95% confidence level for the carriage velocity, turbine rotational speed and torque are defined in Table 2.

Table 2
Experiment data standard deviation and standard error.

	Standard deviation	Standard error
Carriage velocity (m/s)	0.13	±0.008
Rotational speed (rpm)	2.45	±0.1
Torque (Nm)	0.02	±0.001

3.3. Brake calibration

The hysteresis brake controlled the rotational speed of the turbine based on the amount of voltage supplied. The voltage and current have a linear relationship and the relationship of either to the resulting torque is linear above approximately 2.5 V as shown in Fig. 7 below. Since it was easier to regulate the voltage than the current, a control box with a trigger mechanism was used to regulate the voltage supplied to the brake for each run. Hence, voltages were regulated between 2.5 V and the maximum voltage of 5 V by increasing the voltage in each case.

3.4. Towing tank tests

The aim of the tests was to investigate the performance of the Hydro-Spinna turbine at four different depths of immersion. The range of immersions tested was as described in Table 3 and shown in Fig. 8.

The water depth from the bottom of the tank to the shaft centre of the turbine was 470 mm. At a turbine immersion level of 0.36D, the total water depth in the tank was 900 mm. The depth of tip immersion was changed by draining the water out of the towing tank maintaining a constant level of water between the turbine and the bottom of the tank.

4. Test results and analysis

4.1. Energy conversion theory

The power generated by the turbine is defined in the non-dimensional power coefficient. Similarly, the thrust coefficient describes the thrust experienced by the whole system as listed in equations (6) and (7). The performance of turbine is generally presented in plots represented by these coefficients against the tip speed ratios (TSR). TSR is defined as the ratio of the angular velocity at the blade tip to the axial flow velocity as given in equation (8).

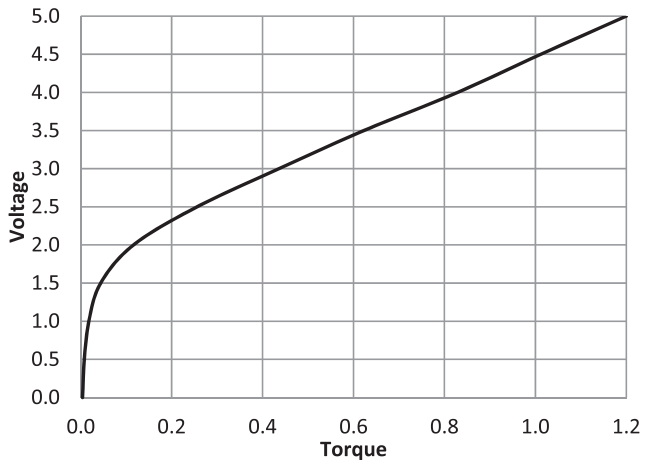

Fig. 7. The voltage and torque relationship of the hysteresis brake calibrated with increasing voltage.

Table 3
Range of immersion depth of the towing tank test.

Immersion depth	Distance (turbine tip to water surface)
0.36D (submerged)	180 mm
0.2D (submerged)	100 mm
0.0D (submerged)	0 mm (Blade tip at the water surface)
−0.5D (partially submerged)	−250 mm (half of the turbine is underwater)

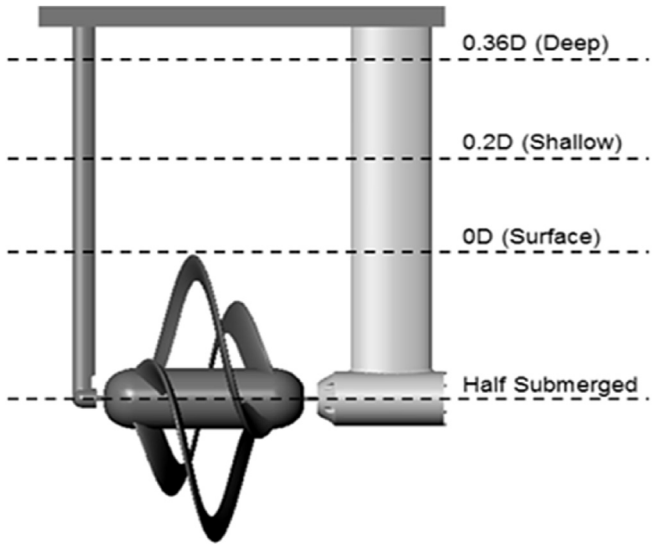

Fig. 8. Illustration of different depth of immersion for the test.

$$\text{Power Coefficient } C_P = \frac{Q\Omega}{0.5\ \rho A U^3} \tag{6}$$

$$\text{Thrust Coefficient } C_T = \frac{T}{0.5\ \rho A U^2} \tag{7}$$

$$\text{Tip Speed Ratio TSR} = \frac{R\Omega}{U} \tag{8}$$

where ρ is the density of the fluid, R is the turbine radius, A is the swept area of the turbine, U is the flow velocity, T is the thrust, Q is the torque and Ω is the angular velocity.

4.2. Test results and discussions

The power coefficient of the turbine at fully submerged level of tip immersion 0.36D is presented in Fig. 9(a). The graph shows the limitation set by the 1Nm brake in getting the full speed range for velocities higher than 0.5 m/s. The turbine produce a maximum power coefficient of 0.275 at an optimal TSR of 2.2. The power performance of the Hydro-Spinna is lower than conventional horizontal axis tidal turbines where a contra-rotating turbine might typically generate a power coefficient of about 0.45 between TSR of 4 and 8 [23]. In another study conducted [9] the performance of the 800 mm diameter tidal turbine generated similar power coefficients with a maximum of 0.46 at TSR of about 6.

The range of the operational tip speed ratio of the Hydro-Spinna model is lower than that of common horizontal axis turbines where operational tip seed ratio is up to a maximum value of 12. The range of operation of the Hydro-Spinna reaches a maximum of just below TSR = 4. Although this seems to be a major disadvantage at the outset the higher blade efficiency may not be the most important criteria for tidal turbines designed to operate for geographical areas with higher tide velocities. In contrast, the low operational TSR range of the Hydro-Spinna indicates that the turbine operates optimally at a much lower rotational speed compared to a conventional tidal current turbine [14,24,25]. This will be an important advantage for removing the possible risk of cavitation and hence associated erosion damage on the blade sections as well as reducing the level of underwater radiated noise that could disturb the marine environment.

It is also observed that the Hydro-Spinna does not require high fluid velocity to overcome its starting torque where it takes a minimum flow of 0.15 m/s for the turbine model to start operating. Even though the Hydro-Spinna doesn't extract as much power as a conventional tidal turbine, its low start up flow velocity makes it operable at speeds below those at which conventional turbines usually start generating. Hence, it is capable of generating power over a longer duration than a conventional turbine. In addition higher blade efficiency may not necessarily be the prime importance for turbines operating in relatively high tidal velocities and designed based on the stall regulation.

The drag of the whole system includes the thrust subjected on the turbine and the supports by the fluid flow. The drag coefficient of the whole turbine system was measured and is presented in Fig. 9(b) and defined in equation (9).

$$C_D = \frac{D}{0.5\rho A_B U^2} \tag{9}$$

where D is the drag force and A_B is the projected area of the system perpendicular to the flow direction.

The results show a decreasing trend in the drag coefficient and hence thrust as the rotational speed of the turbine increases. The drag coefficient is the highest at the tip speed ratio where the turbine starts to rotate and as the tip speed ratio increases, the drag coefficient decreases.

The decreasing drag coefficient of the Hydro-Spinna with increasing TSR (or reducing flow speed) demonstrates a contrasting observation in the thrust coefficient trend produced by other horizontal axis tidal current turbines. Generally, the thrust on the tidal turbine increases with the rotational speed as presented in other studies [9,24,26,27]. For comparison, the thrust coefficient on a common horizontal axis turbine is extracted from Luznik [24] and reproduced in Fig. 10 but note that this turbine operates over a higher TSR range than the Hydro Spinna. The distinct drag coefficient profile of the Hydro-Spinna may be due to the nature of the turbine itself as it is extended in the axial dimension. The blade pitch angle in the front half of the turbine is positive, while the pitch angle of the rear half of the turbine is negative, where the direction of the resultant velocity seen by each half will be different. It is suggested that the trend is produced due to the interactions of the resultant forces on the blades of the Hydro-Spinna. The behaviour of the drag coefficient needs to be further investigated. The decreasing drag indicates a lower loading mooring system can be employed for the Hydro-Spinna turbine, which is likely to be a floating device, than the equivalent conventional device.

The performance of the turbine at 0.36 immersion level was compared against the half submerged performance as shown in Fig. 11; the results present a unique finding in the performance of the turbine when the turbine is half submerged. At half submerged condition the Hydro-Spinna was found to generate half the power of that at the 0.36D immersion level. However, the Hydro-Spinna is only extracting power from half of the turbine swept area hence the power coefficient is 5.5% higher at a TSR of 2.25 than when the turbine was fully immersed at 0.36D. Where in the former case, the

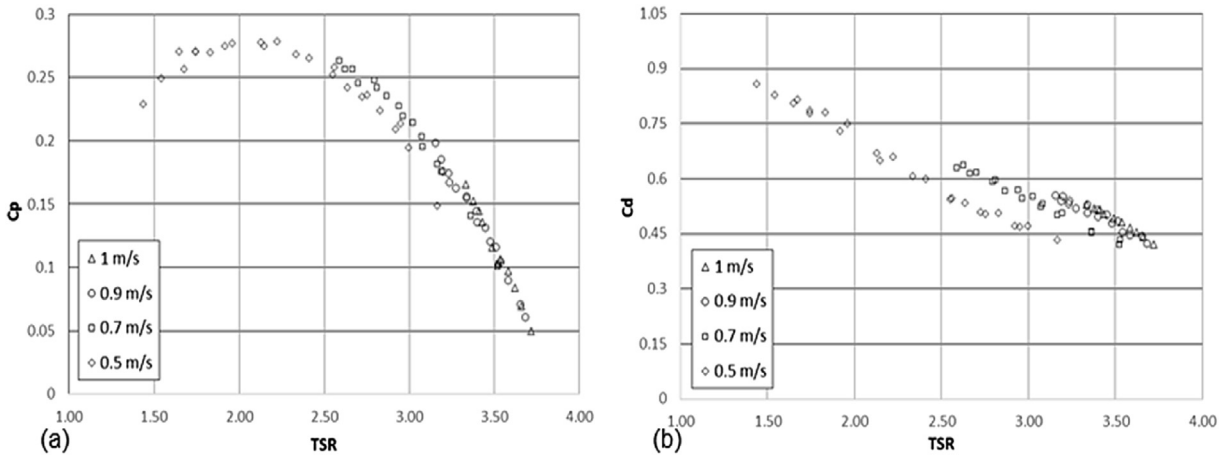

Fig. 9. Performance of the Hydro-Spinna (a) power coefficient and (b) drag coefficient at flow velocities from 0.5 up to 1 m/s.

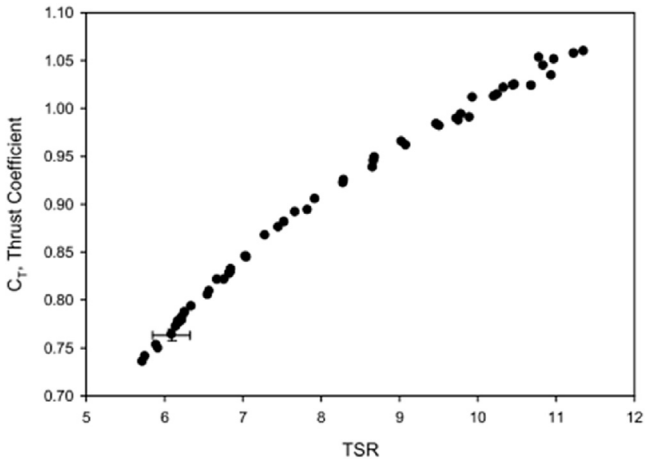

Fig. 10. Thrust coefficient profile for a NACA 63-618 three bladed horizontal axis turbine showing the increasing trend of the thrust coefficient with TSR [24].

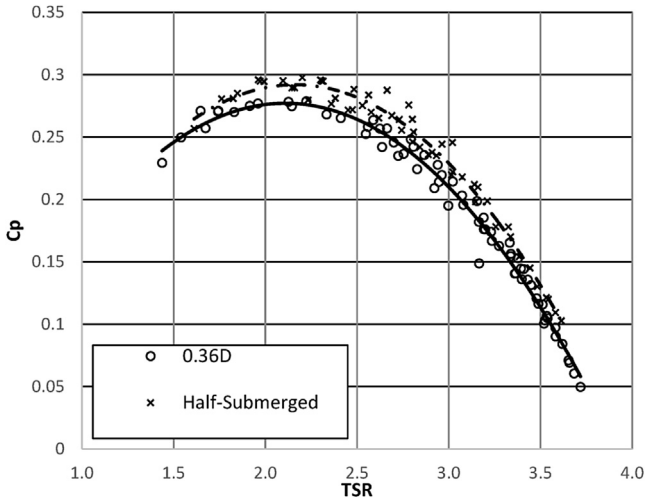

Fig. 11. Power coefficient of the Hydro-Spinna turbine at different flow velocity at deep immersion and half submerged condition.

power available in the flow is calculated only for the area of the turbine which is submerged in the water i.e. half of the turbine area. The power available in the air for the section of the turbine above the water level is assumed insignificant and its contribution neglected in the calculation.

The performance of the Hydro-Spinna at shallow immersion and in the half submerged condition was also compared, as shown in Fig. 12(d). The performances of the Hydro-Spinna in both cases are graphically identical with only a shift of the tip speed ratio operation in the half submerged case.

When the turbine is located right below the water surface, the close proximity of the surface does not affect the performance of the turbine significantly. In the surface condition, the Hydro-Spinna generated a higher power coefficient at higher TSR than for the 0.36D case, as shown in Fig. 12(b). However, as the turbine is close to the surface, the turbine blade appears to cut through the downstream disturbance from the front strut generating obvious surface vortices. This effect is more apparent at low tip speed ratios as the slowly rotating turbine cuts across the disturbances and the generation of vortices is more prominent.

It was observed that the front strut seemed to cause more disturbances downstream to the flow rather than the turbine operation itself and this ultimately disturbed the flow seen by the turbine, as shown in Fig. 13(a). The front strut distorted the unperturbed profile of the flow approaching the turbine as well as creating a surface wave. In fact due to the immediate proximity of both, the turbine in fact saw the turbulent and downstream wake of the front strut. As shown in Fig. 9(b), as the flow velocity increases and hence Reynold's Number, the drag coefficient on the whole system also increases. The turbulence in the flow crucially increased the thrust experienced by the turbine and overall drag on the system as the flow velocity increases. The combined effect of the front strut wake and rotation of the turbine created vortices on either side of the downstream flow.

This phenomenon is more obvious with decreasing immersion depth especially at low tip speed ratio. As presented in Fig. 13(b), the slowly rotating turbine cut across the wake created by the front strut i.e. point X, creating visible surface vortices on either side of the downstream flow i.e. points V. The power performance of the Hydro-Spinna was affected at low tip speed ratio for the surface condition with the power coefficient being lower than anticipated due to the vortices generated.

The disturbance caused by the front strut can be minimized by employing a more streamlined profile to minimise the disturbance or even removing the attachment entirely. However, an installation of the turbine in practice would potentially require a similar arrangement and therefore the experimental results are

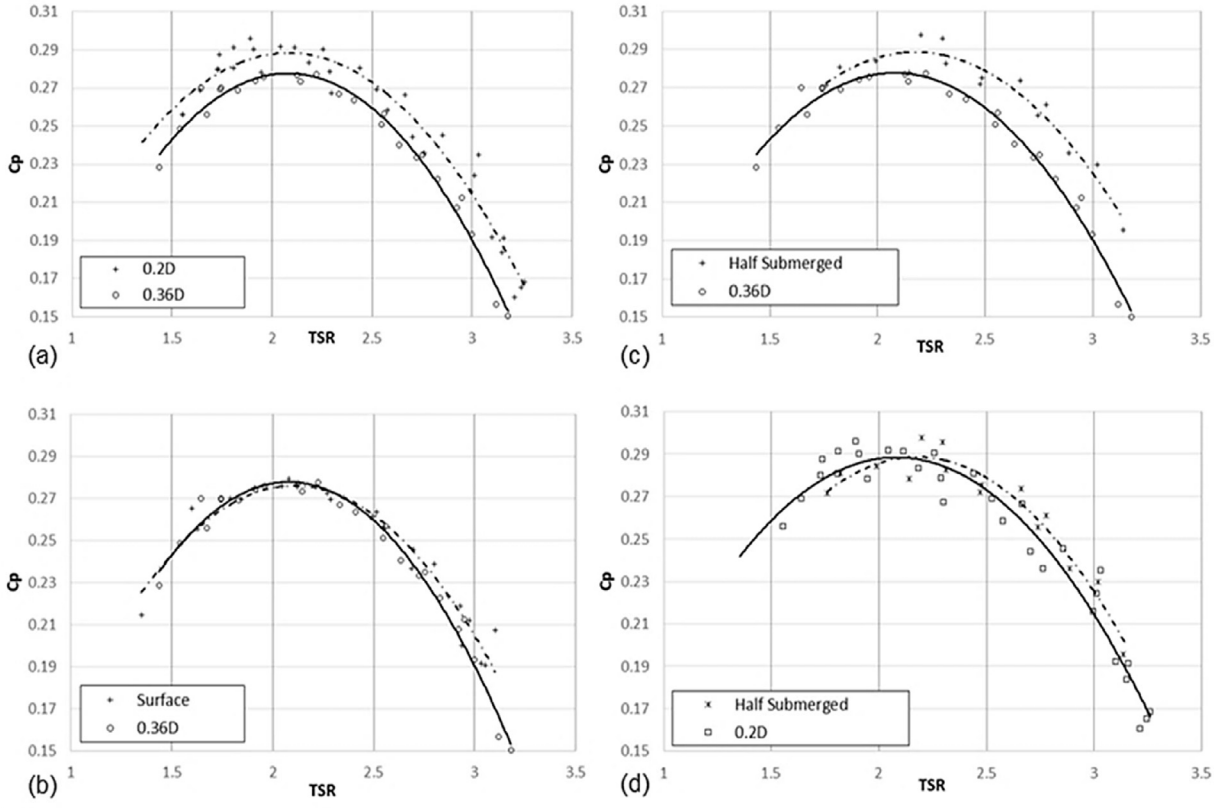

Fig. 12. The power performance graph of the Hydro-Spinna at different immersion depths.

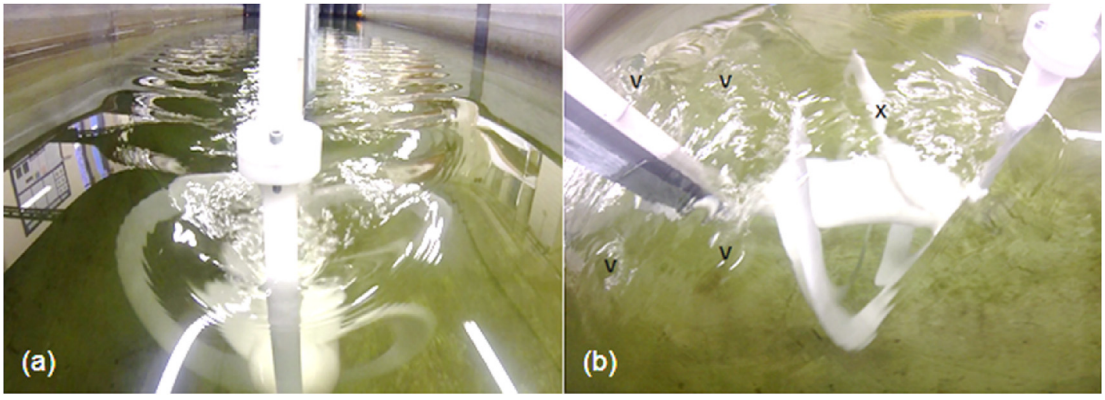

Fig. 13. The Hydro-Spinna turbine during testing just below the surface condition (a) The wake generated downstream of the system (b) Point X where the turbine cuts across the wake of the front strut creating surface vorticity downstream.

representative of the operation of the turbine in a real situation. As it may be considered as an integral part of the system even in full scale application, the effect of the front strut on the performance of the Hydro-Spinna could be investigated in the future.

The increased performance of the Hydro-Spinna with decreasing immersion depth presents a unique result as conventional horizontal axis tidal current turbines produce lower power coefficient as the immersion depth reduces [9,14]. Furthermore, the Hydro-Spinna is found to be operable in the half submerged condition. Not only does the Hydro-Spinna performance improve with decreasing depth of immersion, but its ability to generate power under such conditions merits further investigation of the flow profile across the turbine as well as the wake profile downstream of the turbine. The immediate practical implications of the above findings can be the potential of near surface or in surface locations of such devices that could offer huge savings in terms of logistics and maintenance related costs.

5. Conclusions

A novel horizontal axis tidal current turbine called "*Hydro-Spinna*", was introduced and its operations and performance were investigated based on the scaled model tests conducted in the Newcastle University towing tank. The new concept turbine has interesting features including its adaptability to operate in shallow waters and even in partially submerged conditions. The model tests

were aimed at investigating the power performance of the Hydro-Spinna at different immersion depths as well as to collect data to support computational modelling for developing the concept further.

Based on the investigations it was found that:

- The power coefficient of the current model Hydro-Spinna varied between 0.275 and 0.3 at an optimum TSR of 2.2 for the deeply submerged condition and shallow submerged condition, respectively. These values are low compared to the power coefficient of typical conventional horizontal axis turbines (HAT).
- However, in contrast to conventional HATs, the power coefficient of the Hydro-Spinna displayed an increasing trend with decreasing depth of submergence. It was also interesting to note that the turbine can operate at a partially submerged condition with a power coefficient higher than in the fully submerged condition.
- The drag forces acting on the Hydro-Spinna also displayed an opposite trend to the drag characteristics observed with conventional HATs. As the TSR increased the drag force coefficients were reduced.
- The maximum power coefficients were observed at lower TSR (e.g. around 2.2) as opposed to typically higher TSR values for conventional HATs
- Optimal operations at smaller TSRs and hence rotational speeds suggest remote risk of cavitation and the associated undesirable effects of blade erosion and underwater radiated noise
- The Hydro-Spinna also displayed earlier starting characteristics compared to typically higher values of conventional HAT's
- Despite relatively lower power coefficients, which can be increased further by numerical optimization, the Hydro-Spinna concept may offer greater flexibility for operations at shallower water depths and even in free surface conditions and hence provides improved prospects for logistic and maintenance cost savings in addition to the easy starting of the device and potentially low impact on marine environment.

Acknowledgements

Authors would like to thank Michael Gilbert the designer of the Hydro-Spinna for his contribution to this work. The first author would also like to thank the Brunei Darussalam High Commission for funding her study.

References

[1] EMEC. European Marine Energy Centre 2013;2013. http://www.emec.org.uk/marine-energy/tidal-devices/(accessed March 1, 2015).
[2] A. Baker, Tidal Power, Peter Peregrinus Ltd, 1991.
[3] P.L. Fraenkel, Marine current turbines: pioneering the development of marine kinetic energy converters, Proc. Inst. Mech. Eng. Part A J. Power Energy 221 (2007) 159–169, http://dx.doi.org/10.1243/09576509JPE307.
[4] H. Aly, State of the Art for Tidal Currents Electric Energy Resources, 2011, pp. 1119–1124.
[5] R.H. Charlier, A "sleeper" awakes: tidal current power, Renew. Sustain Energy Rev. 7 (2003) 515–529, http://dx.doi.org/10.1016/S1364-0321(03)00079-0.
[6] M.O.L. Hansen, Aerodynamics of Wind Turbines, Second, Earthscan, London, 2008.
[7] P.A. Lepper, Significance of Dynamic Variation in Renewable Energy Device Noise to Background Noise Levels under Varying Conditions, 2014, pp. 2–5.
[8] D. Wang, M. Atlar, R. Sampson, An experimental investigation on cavitation, noise, and slipstream characteristics of ocean stream turbines, Proc. Inst. Mech. Eng. Part A J. Power Energy 221 (2007) 219–231, http://dx.doi.org/10.1243/09576509jpe310.
[9] A.S. Bahaj, A.F. Molland, J.R. Chaplin, W.M.J. Batten, Power and thrust measurements of marine current turbines under various hydrodynamic flow conditions in a cavitation tunnel and a towing tank, Renew. Energy 32 (2007) 407–426, http://dx.doi.org/10.1016/j.renene.2006.01.012.
[10] A.H. Birjandi, E.L. Bibeau, V. Chatoorgoon, A. Kumar, Power measurement of hydrokinetic turbines with free-surface and blockage effect, Ocean. Eng. 69 (2013) 9–17, http://dx.doi.org/10.1016/j.oceaneng.2013.05.023.
[11] I.G. Bryden, S.J. Couch, How much energy can be extracted from moving water with a free surface: a question of importance in the field of tidal current energy? Renew. Energy 32 (2007) 1961–1966, http://dx.doi.org/10.1016/j.renene.2006.11.006.
[12] SeaGen Tidal Technology, 2013. http://www.seageneration.co.uk/.
[13] L. Myers, A.S. Bahaj, Wake studies of a 1/30th scale horizontal axis marine current turbine, Ocean. Eng. 34 (2007) 758–762, http://dx.doi.org/10.1016/j.oceaneng.2006.04.013.
[14] L. Myers, A.S. Bahaj, Power output performance characteristics of a horizontal axis marine current turbine, Renew. Energy 31 (2006) 197–208, http://dx.doi.org/10.1016/j.renene.2005.08.022.
[15] A.S. Bahaj, L.E. Myers, R.I. Rawlinson-Smith, M. Thomson, The effect of boundary proximity upon the wake structure of horizontal Axis marine current turbines, J. Offshore Mech. Arct. Eng. 134 (2012) 021104, http://dx.doi.org/10.1115/1.4004523.
[16] Y. Li, S.M. Calışal, Modeling of twin-turbine systems with vertical axis tidal current turbines: Part I—Power output, Ocean. Eng. 37 (2010) 627–637, http://dx.doi.org/10.1016/j.oceaneng.2010.01.006.
[17] S. Kiho, M. Shiono, K. Suzuki, The power generation from tidal currents by darrieus turbine, Renew. Energy 9 (1996) 1242–1245.
[18] B. Yang, C. Lawn, Fluid dynamic performance of a vertical axis turbine for tidal currents, Renew. Energy 36 (2011) 3355–3366, http://dx.doi.org/10.1016/j.renene.2011.05.014.
[19] J.M. Davila-Vilchis, R.S. Mishra, Performance of a hydrokinetic energy system using an axial-flux permanent magnet generator, Energy (2013) 1–8, http://dx.doi.org/10.1016/j.energy.2013.11.040.
[20] H. Lin, Evaluating the Performance of an Innovative Marine Current Turbine Based on "Wind Spinner" Concept, Newcastle University, 2009.
[21] Y. Wen, Optimisation and Experimental Validation of a Novel Marine Turbine Device, 2011. MSc in Marine Engineering.
[22] M. Atlar, Recent upgrading of marine testing facilities at Newcastle University, 2nd Int. Conf. Adv. Model Meas. Technol. E. U. Marit. Ind. (2011) 1–32.
[23] J.A. Clarke, G. Connor, A.D. Grant, C. Johnstone, Des. Test. a Contra-rotating Tidal Curr. Turbine 221 (2007) 171–179, http://dx.doi.org/10.1243/09576509JPE296.
[24] L. Luznik, K.A. Flack, E.E. Lust, D.P. Baxter, Hydrodynamic Performance of a Horizontal axis Tidal Turbine under Steady Flow Conditions, Oceans, Virginia Beach, VA, 2012, pp. 1–4.
[25] C.-H. Jo, J.-H. Lee, Y.-H. Rho, K.-H. Lee, Performance analysis of a HAT tidal current turbine and wake flow characteristics, Renew. Energy (2013) 1–8, http://dx.doi.org/10.1016/j.renene.2013.08.027.
[26] W.M.J. Batten, A.S. Bahaj, A.F. Molland, J.R. Chaplin, Experimentally validated numerical method for the hydrodynamic design of horizontal axis tidal turbines, Ocean. Eng. 34 (2007) 1013–1020, http://dx.doi.org/10.1016/j.oceaneng.2006.04.008.
[27] P.W. Galloway, L.E. Myers, A.S. Bahaj, Experimental and Numerical Results of Rotor Power and Thrust of a Tidal Turbine Operating at Yaw and in Waves, 2011, pp. 2246–2253, http://dx.doi.org/10.3384/ecp110572246.